ECS Transactions, 3 (7) 1151-1162 (2006)
10.1149/1.2355909, copyright The Electrochemical Society

Power Output Improvement of Silicon-Germanium Thermoelectric Generators

Martin Wagner[1], Gerhard Span[2], Stefan Holzer[3],
Vassil Palankovski[1], Oliver Triebl[3], and Tibor Grasser[3]

[1]Institute for Microelectronics, Technische Universität Wien
Gusshausstr. 27–29, A-1040 Vienna, Austria
[2]SAM - Span and Mayrhofer KEG, 6112 Wattens, Austria
[3]Christian Doppler Laboratory for TCAD in Microelectronics
at the Institute for Microelectronics

We present a technology for thermoelectric generators using large area pn-junctions. Thermally generated carriers are separated by the gradient of the built-in potential caused by the pn-junction. The use of these structures for waste heat recovery implies an externally applied temperature gradient in-plane with the pn-junction which causes a current of both electrons and holes from the heated to the cooled side, where electrical contacts are mounted. The device behavior is strongly influenced by the magnitude and the spatial distribution of the generation rate as well as the local transport properties. We present the influence of the alloy composition on the material properties and possibilities to increase the power output by modification of the local material composition. Furthermore, the influence of intentionally implanted gold atoms as additional generation centers is assessed. Effective optimization of thermoelectric generators requires a powerful simulation environment due to the strong correlation of different mechanisms within the device. We present simulation results obtained by the device and circuit simulator MINIMOS-NT working in conjunction with the optimization framework SIESTA.

Introduction

Continuously increasing energy costs lead to a rising demand for alternative energy sources as well as new technologies for their efficient usage. A promising candidate for the near future is the direct conversion from heat to electricity using thermoelectric devices, which is already established in special space and remote environments. The usage of this technology on a broad basis requires more efficient and reliable thermoelectric devices and modules. The future range of applications for these devices covers a great variety of thermal environments (1).

Recent work proposed many different approaches for improving the power output and efficiency of thermoelectric devices. Superlattices take advantage of the strong anisotropy of its material parameters as well as the possibility to tailor thermoelectric

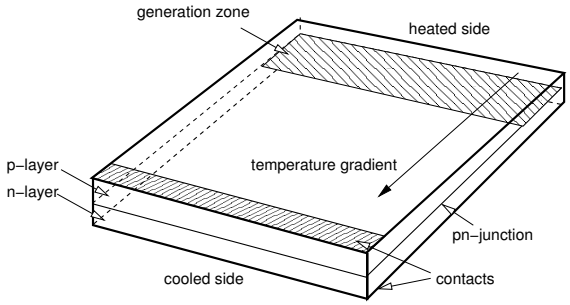

Fig. 1: Large area pn-junction with applied temperature gradient. Thermal generation takes place on the heated side of the structure, both electric contacts are mounted on the cooled side.

emission (2–4). The use of semiconductor nanowires is considered in (5). Several novel materials and material alloys and their thermal and electric transport parameters are inverstigated (6–8).

As of yet, none of these is suitable for a broad economical use. To increase the conversion efficiency, we present a new approach to thermoelectric power generation using large area SiGe pn-junctions (9).

We present the physical background of our approach as well as all necessary material data of SiGe alloys which is explicitely used as a basis for our optimization strategies. We apply our optimization framework SIESTA (10) in conjunction with the device and circuit simulator MINIMOS-NT (11). A rigorous thermodynamical coupling of the heat system with the semiconductor equations is applied as proposed in (12). Finally, we illustrate the impact of our technology with simulation results.

The Approach

A principle sketch of our thermoelectric devices is shown in Fig. 1. Thermal generation of electron-hole pairs takes place on the heated end of the structure. The generated carriers are separated by the gradient of the built-in potential of a large scale pn-junction (Fig. 2). The built-in potential decreases with increasing temperature due to the shifting of the Fermi energy.

A temperature gradient applied along the pn-junction causes a driving force to the free carriers from the hot to the cold part of the structure, a behavior known as the Seebeck effect. The resulting current alters the local carrier balance between

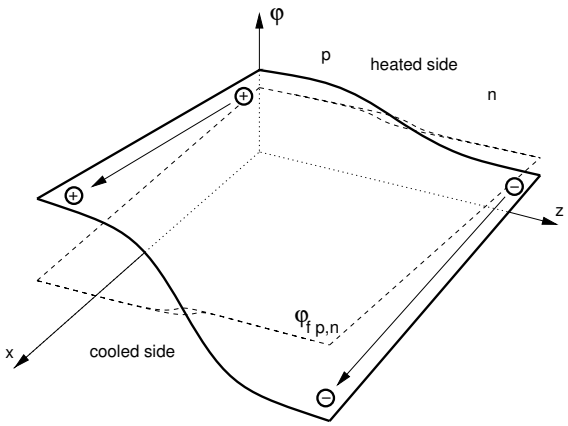

Fig. 2: The electrostatic potential is affected by the local temperature. Higher temperatures lead to smaller energy differences across the pn-junction. The potential change along the x-axis causes a driving force to both carrier types from the zone of strong thermal generation at the hot end to the contacts at the cold end.

generation and recombination and leads to enhanced generation of electron-hole pairs at the hot part and to increased recombination at the cold part of the structure. Contacts at the cooled end of the structure suppress recombination and provide external use of the generated carriers. Hence, this device structure acts as a thermoelectric power source. This principle allows us to use layered structures similar to solar cells as thermoelectric elements. In addition, it could be used to rise the efficiency of solar cells by using non-uniform temperature distributions (13). Thermoelectric modules can be manufactured by stacking these elements, similarly to (14).

Advantages of this technique

The properties of the described assembly are superior to conventional thermocouples in several ways due to the incorporation of the generation of electron-hole pairs. The strong correlation of thermal and electrical properties can be overcome in a wide range because the generation process and the transport of the carriers are spatially separated. The built-in potential gradient of the pn-junction acts as main generation site and separates both carrier types into the corresponding transport layers at the same time. Therefore, the transport properties can be optimized for high electrical conductivity in the n- and the p-layer independently from each other and from the generation properties of the pn-junction. The generation of electron-hole pairs is strongly dependent on the temperature and thus the shape of the temperature gradient has a tremendous influence on the amount of generated electrical current. This correlation opens the possibility to optimize the power density and the conversion efficiency by geometrical engineering and/or by using laterally distributed material

compositions. Since the generation of carriers replaces the need for a direct contact of the n- and p-layer on the hot side, thermoelectric elements can be fabricated using only a single material so fatigue due to thermal cycling can be avoided. SiGe shows high mechanical strength, a high melting point, low vapor pressure, and resistance to atmospheric oxidation, what makes the material attractive for device applications. The elements can be manufactured in a similar way to well established processes in the semiconductor and solar cell industry.

Material Properties of SiGe Alloys

In the following, we present a brief summary of material properties of SiGe alloys and their influences to single mechanisms within the thermoelectric generator. The final power output of the structure depends on a well-suited adjustment of the generation rate, the area of high generation on the heated end of the structure, and the transport properties between the heated side and the contacts applied at the cooled end. The well known Shockley-Read-Hall (SRH) formula is used to calculate the thermal generation and recombination of electron-hole pairs.

Thermal Conductivity

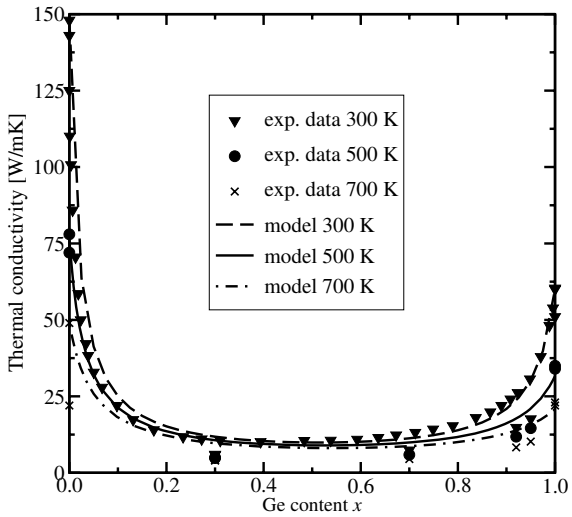

Fig. 3: Thermal conductivity as a function of SiGe material composition at 300 K, 500 K, and 700 K (15). The temperature distribution within a thermoelectric generator can be adjusted by using graded material alloys.

The thermal conductivity decreases with the temperature following a power law

$$\kappa(T_{\mathrm{L}}) \;=\; \kappa_{300}\left(\frac{T_{\mathrm{L}}}{300\ \mathrm{K}}\right)^{\alpha}, \qquad [1]$$

where κ_{300} is the thermal conductivity at 300 K. For SiGe alloys, the thermal conductivity varies between the according values of pure Si and pure Ge following eq. 2 as shown in Fig. 3, the temperature dependence is linearly interpolated between the materials (eq. 3)

$$\kappa_{300}^{\mathrm{SiGe}} \;=\; \frac{1}{\left(\frac{1-x}{\kappa_{300}^{\mathrm{Si}}}+\frac{x}{\kappa_{300}^{\mathrm{Ge}}}+\frac{(1-x)\,x}{C_{\kappa}}\right)}, \qquad [2]$$

$$\alpha^{\mathrm{SiGe}} \;=\; (1-x)\,\alpha^{\mathrm{Si}}+x\alpha^{\mathrm{Ge}}, \qquad [3]$$

with $\kappa_{300}^{\mathrm{Si}} = 148$ W/Km, $\kappa_{300}^{\mathrm{Ge}} = 60$ W/Km, $\alpha_{300}^{\mathrm{Si}} = -1.3$, and $\alpha_{300}^{\mathrm{Ge}} = -1.25$. Here, C_{κ} denotes a bowing factor with a value of 2.8 W/Km for SiGe. The minimum of the thermal conductivity around Ge contents of about 0.5 is used to tailor the temperature distribution and thus the area of high generation rates within the device.

Bandgap

The bandgap continuosly decreases from the value of pure silicon to that of pure germanium. Curves for 0 K, 300 K, and 600 K are presented in Fig. 4. Measurement data is taken from (16–19). The temperature dependence of E_{g} is modeled for each material after Varshni (20) as

$$E_{\mathrm{g}} \;=\; E_{\mathrm{g0}}-\frac{\alpha T_{\mathrm{L}}^{2}}{\beta+T_{\mathrm{L}}}. \qquad [4]$$

For pure Silicon, the bandgap at 0 K is $E_{\mathrm{g0}} = 1.16948$ eV with $\alpha = 4.73\times10^{-4}$ eV/K and $\beta = 636$ K. For pure Germanium, the values are $E_{\mathrm{g0}} = 0.7437$ eV, $\alpha = 4.774\times10^{-4}$ eV/K, and $\beta = 235$ K. For SiGe, the bandgap is derived as

$$E_{\mathrm{g}}^{\mathrm{SiGe}} \;=\; E_{\mathrm{g}}^{\mathrm{Si}}\,(1-x)+E_{\mathrm{g}}^{\mathrm{Ge}}x+C_{\mathrm{g}}(1-x)x \qquad [5]$$

with the temperature-dependent bandgaps of the constituents $E_{\mathrm{g}}^{\mathrm{Si}}$ and $E_{\mathrm{g}}^{\mathrm{Ge}}$ as well as the bowing factor $C_{\mathrm{g}} = -0.4$ eV. The smaller bandgap for high Ge contents is used to optimize the generation rate at the heated side of the structure, the recombination in the other parts is held down with a bigger bandgap.

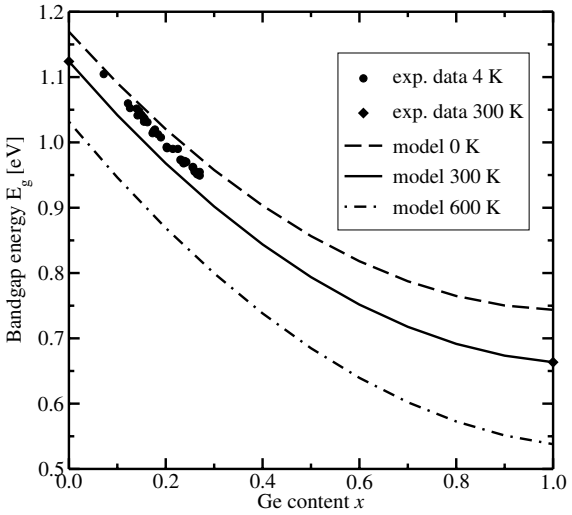

Fig. 4: Bandgap energy as a function of SiGe material composition at 0 K, 300 K, and 600 K. The bandgap energy can be used to maximize the according generation rate and hold down the parasitic recombination rate.

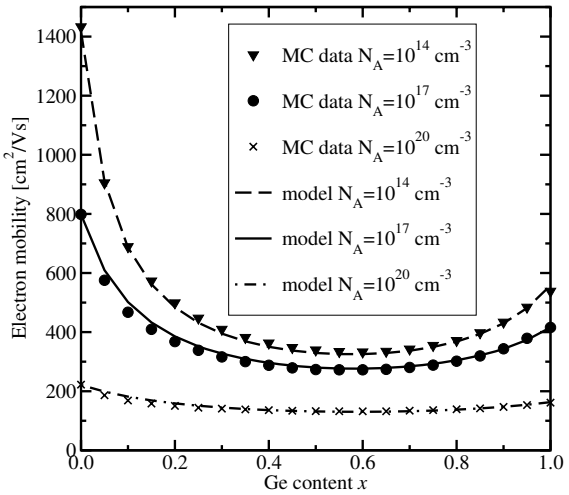

Fig. 5: Electron mobility versus material composition for doping concentrations of $10^{14}\,\mathrm{cm}^{-3}$, $10^{17}\,\mathrm{cm}^{-3}$, and $10^{20}\,\mathrm{cm}^{-3}$ (21). The higher mobility for small Ge contents is used to optimize the conductivity in the transport area of the device structure.

Mobility

The mobility first decreases and then slightly increases for increasing Ge contents (Fig. 5). The power output benefits from higher mobility values in the transport zone between the heated and the cooled side of the device.

Since the thermal conductivity, the bandgap, and the mobility can only be influenced by local adaptions of the Germanium content, strong correlations can be observed between the single material parameters. For example, a Germanium content of about 50% at the cooled side of the structure leads to a shifted temperature curve and thus to large areas of high generation, which is a desired effect. The lower bandgap and mobility at this alloy composition lead to higher recombination and lower mobility, which is contraproductive. The handling of distributed quantities like material composition and additional trap density for optimization yields an enormous number of optimization parameters. In addition, changes in the device geometry require a complete remesh for each evaluation. Since manual optimization for such a large number of parameters is very difficult, we apply the optimization framework SIESTA (10) in order to adjust the power output of our device structures.

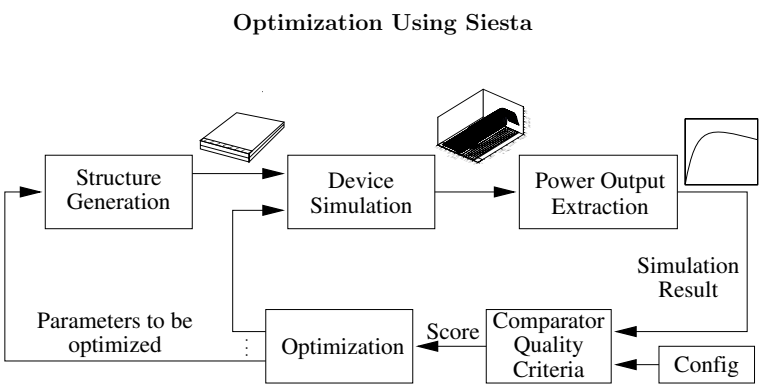

Fig. 6: Principle data flow chart of an optimization run using SIESTA. The single optimization software components are parameterized to our specific problem.

Modern state-of-the-art optimization frameworks offer a wide range of optimization strategies and interfaces to various commercial and tailor-made simulation tools. We use the framework *Simulation Environment for Semiconductor Technology Analysis* (SIESTA) (10), which provides numerous optimizers and interfaces to simulators which can be appropriately chosen and parameterized for a particular class of problems. An overview of the data flow within a SIESTA-controlled optimization is shown in Fig. 6. The core part of the optimization tool flow is the optimizer working in conjunction with an additional tool which compares the simulation result following

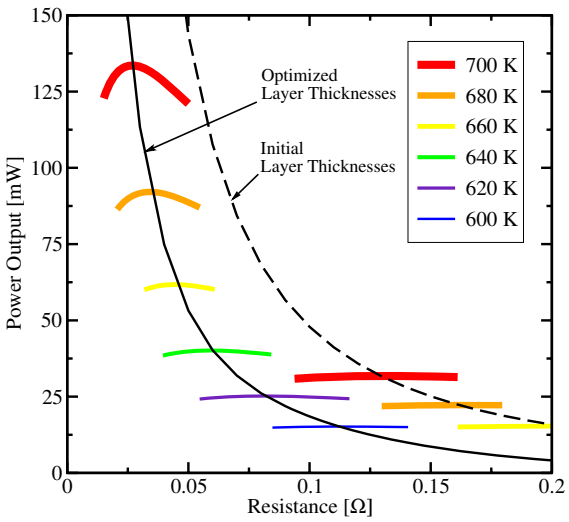

Fig. 7: Power output versus load resistance at different temperatures. Growing temperatures on the hot end lead to higher generation and thus to lower inner resistances. Non-optimum layer thicknesses lead to much lower output at higher inner resistances.

a certain quality criterion. In our case, we maximize the power output of the thermoelectric device structure. The optimizer tries to improve the simulation result by varying the unknown parameters with certain, in general different, strategies in order to optimize the score value and thereby the quality of the power output. Modifications on the parameter vector are based on the simulation quality represented by the score value.

The data processing blocks displayed in the upper half of Fig. 6 symbolically depict the most important parts of typical simulation steps. The block for structure generation represents the geometry definition, dopand distribution, and spatial material composition. Moreover, the generated device structure depends on parameters influenced by the optimizer. The geometrically defined structure is meshed to generate the semicunductor device structure, which is electrically analyzed in the device simulator block by MINIMOS-NT (11). Furthermore, MINIMOS-NT provides all propriate models necessary for the evaluation of the given parameter set. Afterwards, a post processing step extracts the power output versus the load resistance for one certain structure. Finally, a maximum search is performed on these values for one specified given device structure in order to achieve power matching with a load resistance. This obtained matched power output is used as optimization target to be maximized. With the obtained optimal power output, a parameter set for an ideal device structure under given constraints is identified. Different optimization studies for several constraints are presented in the following section.

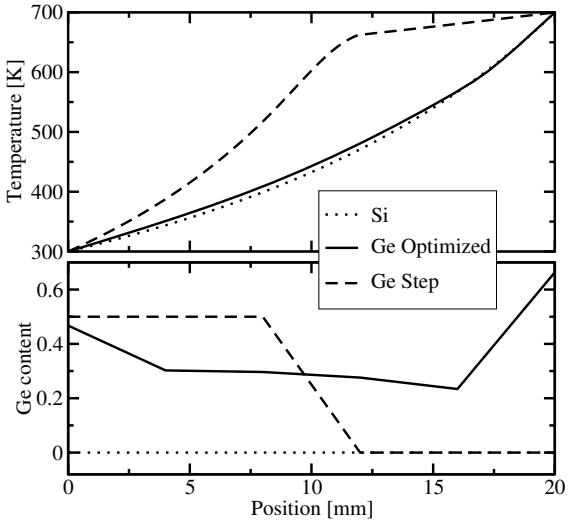

Fig. 8: Temperature distributions for several Ge content profiles. The lower thermal conductivity of Ge leads to shifted temperature curves. The optimum Ge distribution is also affected by the modified bandgap as well as the mobility.

Results

In the following part, several optimization strategies and the resulting power outputs are presented. The generation of electron-hole pairs is a thermally activated process determined by the trap level, the bandgap, and the local temperature. Fig. 7 shows the increase of the power output with respect to the temperature of the heated end. Generation rates increase exponentially with the temperature. As long as effective transport of the additionally generated carriers from the generation zone at the heated end to the contacts at the cooled end is ensured, the power output rises with the temperature. Too low transport layer thicknesses strongly decrease the power output as indicated with the dotted line in Fig. 7. Too thick profiles also increase recombination which means that less carriers reach the contacts. In both cases, the power output is dramatically lower than under ideal transport conditions.

Large areas of high temperature are needed to generate as much carriers as possible but at the same time a temperature gradient is necessary to remove the carriers effectively from the generation zone. We use graded SiGe alloys as shown in Fig. 8 to optimize the local material properties to our needs. As pointed out in Fig. 3, the thermal conductivity drops with increasing Ge content from 0% to 50%. This mechanism is used to control the temperature distribution along the pn-junction and thus the generation rate. Increased Ge content on the cooled side leads to a temperature distribution with a shallow slope at high temperatures and a steep slope

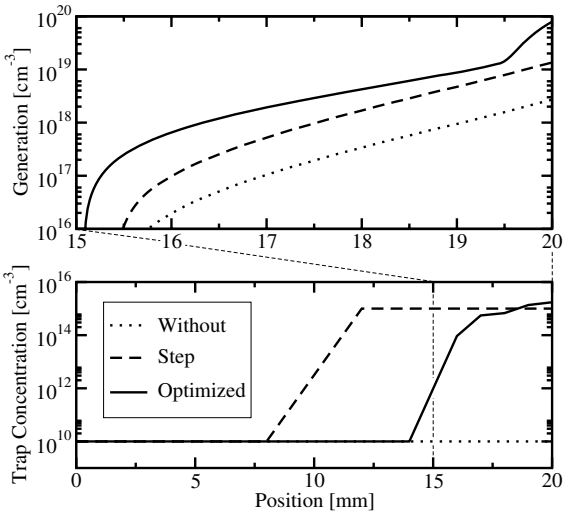

Fig. 9: Thermal carrier generation for different trap concentration profiles. Gold is used as trap material because of its ideal energy level. An optimal trap distribution leads to highest generation rates.

approaching the cooled part of the structure, displayed with the dashed line in Fig. 3. The optimized Ge profile also accounts for the dependence of the bandgap as well as the mobility on the alloy composition. Since the bandgap decreases continuosly from pure Si to pure Ge, strongly increased Ge contents at the heated end of the device lead to a smaller bandgap and thus to higher generation rates. For optimum transport conditions, the mobility in the transport zone between the generation zone at the heated side and the contacts at the cooled end has to be maximized. This can be achieved by intermediate Ge-contents as illustrated in Fig. 5.

Since the modification of local alloy compositions influences the temperature distribution, the mobility, and the bandgap, another mechanism had to be introduced which only affects the generation rate. We have achieved further improvements by the application of an optimized gold dopand profile as additional generation centers (Fig. 9). Gold is used as a trap material because of its ideal energy level in the middle of the bandgap (22). Both the device structure and the doping profile have been adapted accordingly to maximize the amount of generated carriers.

The evolution of the optimization is presented in Fig. 10. The p- and n-doped transport layer thicknesses are optimized for the most effective carrier transport from the high temperature generation area to the contacts (Fig. 1). Non-optimal doping profiles lead to higher recombination rates and thus to lower power output. The power output of the finally optimized structure is 18 times higher than the one of the initial pure Si structure.

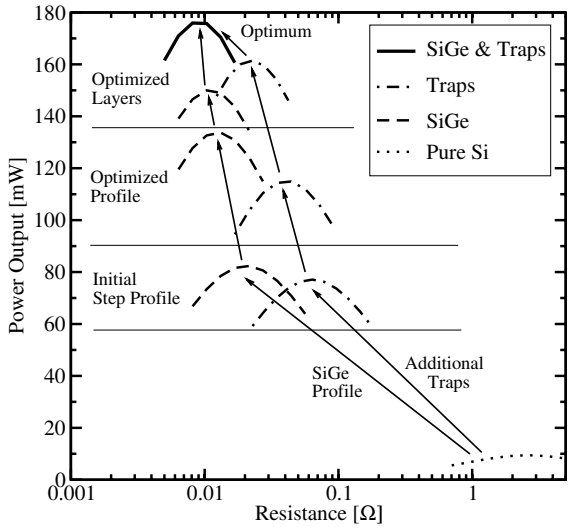

Fig. 10: Power output for several structures in several development states at 700 K hot end temperature. The power output of the final optimized generator design is 18 times higher than the one of a pure Si generator.

Summary and Conclusion

A novel approach to thermoelectric power generation using the thermal generation within large area pn-junctions was presented. Several material parameters of SiGe and their models within the device simulator MINIMOS-NT have been illustrated. Their influence on the spatial distribution as well as the maximum magnitude of the generation rate and the electrical and thermal transport properties have been presented as well as the overall device characteristics. The local alloy composition as well as the spatial distribution of additional dopands as generation centers have been improved using the optimization framework SIESTA in conjunction with MINIMOS-NT to increase the power output of the device. Both the power output and efficiency of the investigated thermoelectric generators shown in Fig. 1 have been dramatically increased.

Acknowledgments

We acknowledge financial support through the FFG, the Austrian Research Promotion Agency (Österreichische Forschungsförderungsgesellschaft) for project no. 809975 (SAM) and project no. 810128 and the local government (Impulspaket Tirol).

References

1. G. Span, M. Wagner, and T. Grasser, *The 3rd European Conference on Thermoelectrics Proceedings ECT2005*, Nancy, France, (2005).
2. D. Vashaee, and A. Shakouri, *J. Appl. Phys.*, **95**(3), 1233 (2004).
3. B. Yang, J.L. Liu, K.L. Wang, and G. Chen, *Appl. Phys. Lett.*, **80**(10), 1758 (2002).
4. S.-M. Lee, and D.G. Cahill, *Appl. Phys. Lett.*, **70**, 2957 (1997).
5. N. Mingo, *Appl. Phys. Lett.* **84**(14), 2652 (2004).
6. S. Yamaguchi, Y. Iwamura, and A. Yamamoto, *Appl. Phys. Lett.*, **82**(13), 2065 (2003).
7. P. Hagelstein, and Y. Kucherov, *Appl. Phys. Lett.*, **81**(3), 559 (2002).
8. M. N. Tripathi, and C. M. Bhandari, *J. Phys. Cond. Matter*, **15**, 5359 (2003).
9. G. Span, Austrian patent AT 410 492 B; international patent application PCT/AT01/00123, granted in USA, Russia, Europe.
10. *SIESTA 1.1std*, Institut für Mikroelektronik, Technische Universität Wien, Austria, (2003).
11. IμE, MINIMOS-NT 2.1 User's Guide, Institute for Microelectronics, Technische Universität Wien, Austria, (2004).
12. G. Wachutka, *IEEE Trans. CAD*, **9**, 1141 (1990).
13. S. Kettemann, and J.-F. Guillemoles, *16th Workshop on Quantum Solar Energy Conversion*, Bad Gastein, Austria, (2004).
14. C.S. Tan, A. Fan, K.-N. Chen, and R. Reif, *7th Annual Topical Research Conference on Reliability*, Austin, Texas, (2004).
15. P. Maycock, *Solid-State Electron.*, **10**(3), 161 (1967).
16. D.J. Robbins, L.T. Canham, S.L. Barnett, A.D. Pitt, and P. Calcott, *J. Appl. Phys.*, **71**(3), 1407 (1992).
17. J. Brunner, J. Nutzel, M. Gail, U. Menczigar, and G. Abstreiter, *Journal of Vacuum Science and Technology B*, **11**(3), 1097 (1993).
18. D. Dutartre, *Physical Review B*, **44**(20), 11525 (1991).
19. J. Spitzer, K. Thonke, R. Sauer, H. Kibbel, H.-J. Herzog, and E. Kasper, *Appl. Phys. Lett.*, **60**(14), 1729 (1992).
20. Y. Varshni, *Physica*, **34**(1), 149 (1967).
21. V. Palankovski, G. Röhrer, T. Grasser, S. Smirnov, H. Kosina, and S. Selberherr *Applied Surface Science*, **224**, 361 (2004).
22. F. Richou, G. Pelous, and D. Lecrosnier, *Journal of Applied Physics*, **51**, 6252 (1980).